Available online at www.sciencedirect.com
SCIENCE DIRECT®
Mathematical Biosciences 188 (2004) 157–174
Mathematical Biosciences
www.elsevier.com/locate/mbs

Coding of information in models of tuberous electroreceptors

Martin St-Hilaire, André Longtin *

Department of Physics, MacDonald Hall, University of Ottawa, 150 Louis Pasteur, Ottawa, ON, Canada K1N 6N5

Received 17 December 2002; received in revised form 11 August 2003; accepted 20 August 2003

Abstract

Weakly electric fish continuously emit a quasi-sinusoidal electric organ discharge (EOD) to probe their near environment (electrolocation). P-type tuberous receptors located on their skin respond to amplitude modulations of the EOD by varying their firing rate. These receptors, and the neuronal circuitry downstream from them, must encode and process low-frequency stimuli due to prey and obstacles and certain communication signals, as well as high-frequency communication signals emitted by other fish. We ultimately seek the biophysics that govern the encoding process, and in particular, the sensitivity to certain stimulus features. Since the pyramidal cells to which these receptors project can also be monitored, studies of weakly electric fish offer a great opportunity for deciphering the encoding/decoding problem. Here we briefly summarize our recent advances on this issue. We then present new results on the encoding properties and relative modeling advantages of two widely used classes of neuron models of electroreceptor activity: a leaky integrate-and-fire dynamical model, and a non-dynamical modulated stochastic point process model. The quality of encoding, based on the stimulus reconstruction method, is assessed as a function of firing rate and stimulus contrast, in the context of bandlimited Gaussian stimuli. Our main conclusion is that the quality of encoding increases strongly with firing rate, but also depends on the actual combination of biophysical parameters that determine this rate.

Keywords: Electric fish; Neuronal coding; Spike generator; Stochastic neuron models; Integrate-and-fire model; P-units; Neuronal noice; Information theory; Electrolocation

* Corresponding author. Tel.: +1-613 562 5800x6762; fax: +1-613 562 5190.
E-mail address: alongtin@physics.uottawa.ca (A. Longtin).

0025-5564/$ - see front matter
doi:10.1016/j.mbs.2003.08.012

1. Introduction

To elucidate the computations accomplished by nervous systems, it is useful to study a preparation in which the activity can be recorded in chains of neurons, starting at the sensory periphery and going centrally. Statements about 'neuronal coding' by one cell can then be verified by recording the activity in the postsynaptic cell. For example, if a study concludes that a primary receptor encodes only the magnitude of upswings in an external stimulus, the postsynaptic neuron better be able to discriminate between different upswings. Another important factor is the complexity of the circuitry, such as the number of cell types in a given nucleus. Such complexity of course impedes our understanding, especially when it prevents the clear identification of input and output for a cell or a cell population. Finally it helps if the stimulus ensemble relevant to the animal is limited. All these factors pose serious difficulties for the study of mammalian brains.

The sensory system of the weakly electric fish offers an excellent opportunity to test statements about neural coding. They produce a weak quasi-sinusoidal electric field (electric organ discharge or EOD) which is modulated in phase and amplitude by stimuli. Here we will focus solely on amplitude modulations (AMs) of the EOD caused by lower-frequency stimuli. These fish have no cortex, which makes their neural circuitry relatively less complicated. The input/output of different stages is well-defined. Further, it is possible to record (1) the external electric field modulations caused by stimuli; (2) the firing activity of the receptor afferents; (3) the activity of their postsynaptic pyramidal cells; and even (4) from the neurons at the next stage in the nucleus preeminentialis. And the relatively simple stimulus ensemble consists of low-frequency bandlimited noise associated with prey and obstacles (such as rocks) and certain communication signals, as well as higher-frequency signals associated with special communication signals (chirps) between fish. Such frequency characteristics are determined by Fourier spectral measurements of the electrical signals caused by such signals, and the low- vs high-frequency label relates to where the dominant power lies (e.g. at low frequencies for so-called low-frequency stimuli). In this study we concentrate on the coding of lower-frequency stimuli by two model classes.

The purpose of the electrosensory system is to 'make sense' of these random AMs of the electric field caused by interesting stimuli, and filter out uninteresting ones. Thus, noisy time-varying stimuli will be of interest here throughout our work. Interestingly, in the absence of stimuli (i.e. of EOD modulations), different receptors have different 'baseline firing rates'. The role of this distribution of baseline rates is not known, and we can speculate about this role using a combination of modeling and information theory calculations.

The goal of this paper is to present such calculations, and provide clues for the role of the baseline firing rate (calculated as a probability of firing per EOD cycle, or '*P*-value') and of the noise seemingly present in these receptors. The two classes of models we focus on are well-grounded in the biomathematics literature, and reveal different aspects of the coding process in P-type electroreceptors, which we will refer to as P-units. Both involve noise at a basic level, which appears as a plausible ingredient of the dynamics of these receptors. Our study reveals the relative advantages of the two model classes in the context of a specific coding problem.

The paper is organized as follows: A description of the electric fish and of their electroreceptors is given in Section 2. Sections 3–5 consider a dynamical integrate-and-fire framework for modeling P-unit activity, and presents results on coding in this model. Section 6 considers a modulated

point process model of their firing activity. It was developed by Nelson et al. [13], and is extended here to reveal certain aspects of the coding capabilities of the P-units as a function of their firing statistics. A discussion follows in Section 7. While our results are developed in the context of electroreception, they are relevant to cells driven by a carrier signal (such as the EOD) which is modulated by environment stimuli, as occurs e.g. in auditory systems.

2. What are P-units?

A comprehensive survey of the known anatomy and physiology of the electrosensory system of the weakly electric fish of interest here (*Apteronotus leptorhynchus*, or *AL*) can be found in Ref. [20]. This weakly electric fish probes its environment via active electrolocation, see e.g. [1]. The quasi-sinusoidal EOD from the tail area has a precisely controlled frequency between 0.6 and 1.0 kHz. The EOD produces a time-varying potential on the fish's skin. There, tuberous electroreceptors respond to modulations of this potential by varying their firing rate.

Spiking activity in these receptors is phase locked to the EOD [12,14,16], in the sense that firings always occur within a certain EOD phase interval and at most once per cycle. Consecutive action potentials are separated in time by roughly a random integer number of EOD cycles. This behavior is called 'skipping'. Each receptor has a P-value, which is the probability that it triggers a spike at each EOD cycle in the absence of a stimulus, i.e. in the presence of the baseline EOD alone. It is observed that the P-value is a smoothly increasing function of the EOD amplitude [16]. Accordingly, 'probability' or P-type coders – in contrast with time or T-type coders which trigger a spike every EOD cycle – encode carrier (EOD) amplitude modulations (AMs) by varying their skipping pattern. The EOD can be perturbed by nearby objects (rocks, worms) with an impedance different from that of the surrounding water. Their refractory period prevents them from firing more than once per EOD cycle.

Only extracellular recordings of spikes from P-units are presently possible. The precise mechanisms of synaptic transmission and of firing are not known. Thus we rely on indirect evidence from other preparations and on numerical calculations and mathematical models to understand P-unit firing. Earlier work has revealed that a population of these receptors shows a wide range of values of P – even within the same specimen for which the EOD frequency is constant [12]. The question of the role for this distribution thus arises. In this paper, the biophysical determinants of P are considered, along with the possible role of P from the information theory point of view.

A single P-type electrosensory unit consists in tens of individual receptor cells grouped at the base of an epidermal pit [1]. Each of the receptor cells releases neurotransmitter to an afferent nerve that innervates the whole unit and triggers an action potential when the stimulation reaches a given threshold. Neurotransmitter release rate and conductance are generally known to be unreliable – or 'noisy' – during the synaptic transmission process. Hence, it is strongly believed that the synaptic transmission process at the release sites, given their large number and their associated unreliability, is responsible for most of the noise (and skipping) in the encoding process in P-units [2,13,15,18].

3. Methods

For both models studied in this paper, the input stimulus, which is an AM of the EOD, was generated by filtering Gaussian white noise with a fourth-order low-pass filter, similarly to what was done in [11]. The only difference is that the input to this filter was Ornstein–Uhlenbeck noise in that work, while here it is zero-mean Gaussian white noise $\xi_{\mathrm{st}}(t)$ with autocorrelation $\langle \xi_{\mathrm{st}}(t)\xi_{\mathrm{st}}(s)\rangle = 2D_{\mathrm{st}}\delta(t-s)$, where δ is the Dirac delta function. The subscript 'st' refers to the fact that this white noise produces the stimulus signal, i.e. realistic AMs of the EOD. The equations for this filter are

$$\frac{\mathrm{d}S}{\mathrm{d}t} = z_2, \tag{1}$$

$$\frac{\mathrm{d}z_2}{\mathrm{d}t} = z_3, \tag{2}$$

$$\frac{\mathrm{d}z_3}{\mathrm{d}t} = z_4, \tag{3}$$

$$\frac{\mathrm{d}z_4}{\mathrm{d}t} = 4\alpha z_4 - 6\alpha^2 z_3 + 4\alpha^3 z_2 + \alpha^4[-S(t) + \xi_{\mathrm{st}}]. \tag{4}$$

These AMs have a well-defined upper cutoff frequency given by $\alpha/2\pi$, which we set at one-tenth of the EOD frequency [16], i.e. $\alpha = 2\pi/10$ ($f_{\mathrm{EOD}} = 1$, corresponding to 1 kHz). This noise modulates the amplitude of a sinusoidal signal (i.e. of the EOD). The value of D_{st} was chosen to yield a standard deviation of the resulting AM signal $S(t)$ equal to 17% of the mean EOD amplitude r_0, i.e. $\sigma_{S(t)} = 0.17$.

Further, a separate Gaussian white noise ξ_{syn} was added to the amplitude of the EOD to mimick synaptic noise (see below). A refractory period was numerically implemented to prevent the occurrence of unrealistically close spikes. From the input analog signal $S(t)$ and the output digital spike train, a linear estimate $S_{\mathrm{est}}(t)$ of the stimulus $S(t)$ was computed using the optimal Wiener–Kolmogorov filter $h(t)$ [8,16,21]:

$$h(t) = \int_{-f_{\mathrm{c}}}^{f_{\mathrm{c}}} \mathrm{d}f \, \frac{S_{sx}(-f)}{S_{xx}(f)} \mathrm{e}^{-\mathrm{i}2\pi f t}, \tag{5}$$

where f_{c} is the cutoff frequency (or 'bandwidth') of the input signal. This filter minimizes the reconstruction noise defined below. The quantities $S_{sx}(f)$ and $S_{xx}(f)$ are, respectively, the cross-spectrum between $S(t)$ and the spike train, and the auto-spectrum of the spike train. The estimate $S_{\mathrm{est}}(t)$ was computed by convolving the delta functions making up the spike train with $h(t)$. The difference $n(t) \equiv S_{\mathrm{est}}(t) - S(t)$ is usually referred to as 'noise' in this information theory literature. Here we will refer to it as 'reconstruction noise', to distinguish it from the noise used in the model dynamics (synaptic noise) and the input signal (the random amplitude modulation, or 'AM'). This is important since in dynamical models, it is possible to e.g. decrease reconstruction noise by increasing synaptic noise, through the stochastic resonance effect [11]. We use the coding fraction

$$\gamma = 1 - \frac{\epsilon}{\sigma_{S(t)}}$$

as a measure of information transmission [16], where ϵ is a measure of the noise power:

$$\epsilon^2 = \int_{-f_c}^{f_c} \mathrm{d}f S_{nn}(f) \tag{6}$$

and S_{nn} is the power spectrum of $n(t)$. Also, $\sigma_{S(t)}$ is the standard deviation of $S(t)$, and thus, $0 \leqslant \gamma \leqslant 1$. A higher value of γ implies better coding, since $S(t)$ can then be better reconstructed from the knowledge of the spike train.

4. Dynamical model of P-unit firing

4.1. Model

The standard leaky integrate-and-fire neuron model was adapted by Chacron et al. [2] to reproduce the first-order as well as certain second-order firing statistics of P-units. Its deterministic properties have been analyzed in Chacron et al. [4]. The key element of this model is a dynamic threshold variable which preserves a memory of the recent firing history, as seen in the autocorrelation function of successive interspike intervals which show a negative correlation at lag one (not shown). The leaky integrate-and-fire model with dynamic threshold (LIFDT) model is basically an LIF model with a threshold $\omega(t)$ that changes in time and obeys the following rule: When the potential $v(t)$ equals the threshold $\omega(t)$, a spike occurs, and the threshold is raised from its current value by a fixed quantity $\Delta\omega$. It then decays exponentially towards a 'rest' value ω_0 after an absolute refractory period T_{ref}. The threshold tends to increase when a few firings occur in a small time window, thus making the following interval more likely to be longer. Similarly, a long interval will allow $\omega(t)$ to recover more, making a short interval more probable. As for $v(t)$, it is reset to zero after the spike and resumes its evolution as in the usual LIF model. These considerations lead to the following equations:

$$\dot{v} = \frac{v_0 - v}{\tau_v} + i(t)\frac{i(t)}{C}, \tag{7}$$

$$\tau_\omega \dot{\omega} = H(t - t_{\mathrm{last}} - T_{\mathrm{ref}})(\omega_0 - \omega) + \Delta\omega\delta(t - t_{\mathrm{last}}), \tag{8}$$

where the post synaptic current $i(t)$ is coupled additively to the current balance equation and δ is the Dirac delta function. The refractory period is implemented by the Heaviside function $H(\cdots)$ with t_{last} being the time of the last spike. The capacitance C was set equal to 1.

The input current $i(t)$ is determined by the EOD and synaptic properties such as rectification and noise $\xi(t)$. The former accounts for the fact that many synapses in receptors respond to only one polarity of an input signal [5,6,10]. This is simply realized by setting to zero all parts of the forcing that correspond to negative values of the sinusoid. Hence the forcing term $i(t)$ of Eq. (7) is written as

$$i(t) = r_0[1 + S(t) + \xi_{\mathrm{syn}}(t)]\sin(\beta t)H[\sin(\beta t)] + \eta(t). \tag{9}$$

Here r_0 is the mean EOD amplitude. The signal $S(t)$ is defined in Eq. (4); note that this AM multiplies the mean amplitude r_0. The EOD angular frequency is given by $\beta \equiv 2\pi f_{\mathrm{EOD}}$, with f_{EOD} set to equal to 1 in our paper. The Gaussian white noise $\xi_{\mathrm{syn}}(t)$ has zero mean and correlation function $\langle \xi_{\mathrm{syn}}(t)\xi_{\mathrm{syn}}(s)\rangle = 2D_{\mathrm{syn}}\delta(t-s)$; we refer to $\sigma^2 \equiv 2D_{\mathrm{syn}}$ as its variance. It is meant to represent synaptic noise. Some plots below are given for two distinct values of σ^2. This noise is constant during one EOD cycle, and jumps to a new value at the next EOD cycle. Qualitatively similar results have been obtained using Gaussian white noise (not shown).

The other additive noise source $\eta(t)$ is an Ornstein–Uhlenbeck process with correlation time τ_{add}:

$$\tau_{\mathrm{add}} \frac{\mathrm{d}\eta}{\mathrm{d}t} = -\eta + \xi_{\mathrm{OU}}(t), \tag{10}$$

where the intensity of the Gaussian white noise ξ_{OU} is $2D$. The variance of the OU noise is given by $\sigma^2_{\mathrm{add}} = D/\tau_{\mathrm{add}}$. Its effect is mainly to add more phase jitter and other more subtle correlation effects in the firing data [3]. It widens the modes in the interspike interval histograms (ISIH). For all simulations, the cutoff frequency was set to 100 Hz, and the 'constant contrast' amplitude of the signal was chosen so that its standard deviation was always $0.15r_0$, based on [16]. Time is in milliseconds.

4.2. Firing characteristics

We present various aspects of the response from LIFDT to noisy and/or periodic input, and the dependence of the P-value on certain important parameters. All our simulations use the parameters: $v_0 = 0.0$ mV, $\omega_0 = 0.03$ mV, $\Delta\omega = 0.05$ mV, $\tau_v = 1.0$ ms, $\tau_\omega = 7.75$ ms, $T_{\mathrm{ref}} = 1.0$ ms, $\beta = 2\pi$ (corresponding to a 1 kHz EOD), $D = 1.758 \times 10^{-4}$ (additive noise intensity), and $\tau_{\mathrm{add}} = 0.075$ ms. We verified that this simplification minimally affected our measures of information transfer. For these values, the deterministic baseline firing (i.e. for constant EOD amplitude) shows a 5:1 periodic pattern – one spike occurs every 5 EOD cycles and $P = 0.2$. A sample time course of the voltage and threshold variables for this phase locked pattern is illustrated in Fig. 1(left). In this regime, the dynamics are suprathreshold since action potentials can occur without the presence of synaptic noise or an AM.

With noise ($\sigma^2 = 0.0256$), the periodic 5:1 pattern is perturbed. As a result, skipping occurs (Fig. 1(right)) leading to ISIHs and interval serial correlations matching those seen in experiments (not shown, see [2]). The ISIH envelope is bell-shaped, with discrete modes spread over a few EOD periods with a mean of 5 cycles.

The model behavior in response to AMs is shown in Fig. 2 along with the principal signals involved in the simulations. The top signal (A) represents the stimulus that is to be encoded through modulation of the fish's EOD (B). After rectification of the modulated EOD and addition of noise, integration of the postsynaptic current leads to the typical dynamics of $v(t)$ and $\omega(t)$ shown in (C). Spikes tend to occur at a higher (lower) rate when $S(t)$ is high (low).

Fig. 3 studies the dependence of the P-value on the EOD amplitude in the absence of AMs. As the EOD amplitude increases, P increases (panel A) following a devil's staircase relation [9,19]. Because of phase locking, the same P-value may result from different EOD amplitudes and this is seen as plateaus in an otherwise monotonically increasing function of r_0. Plateaus are expected to

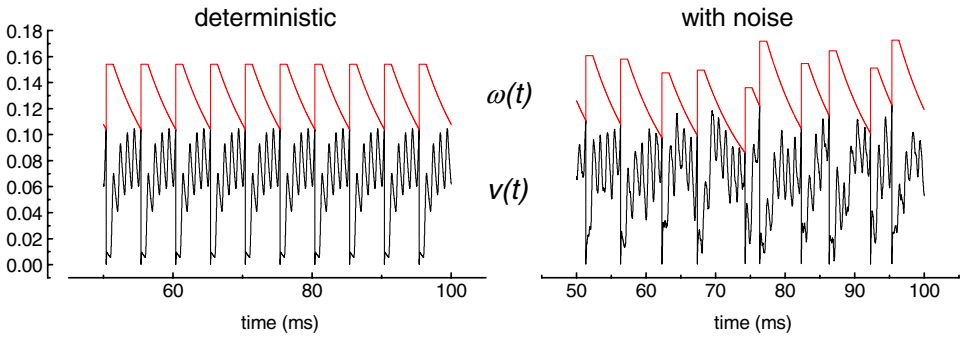

Fig. 1. Effect of noise on LIFDT dynamics. (Left) Periodic response from constant amplitude forcing, without additive ($D = 0$) and synaptic ($\sigma^2 = 0$) noise, and without AM ($\sigma_{S(t)} = 0$). Here the mean amplitude of the EOD is $r_0 = 0.261$. (Right) The response is no longer periodic when perturbed by the presence of non-zero synaptic noise intensity ($\sigma^2 = 0.0256$).

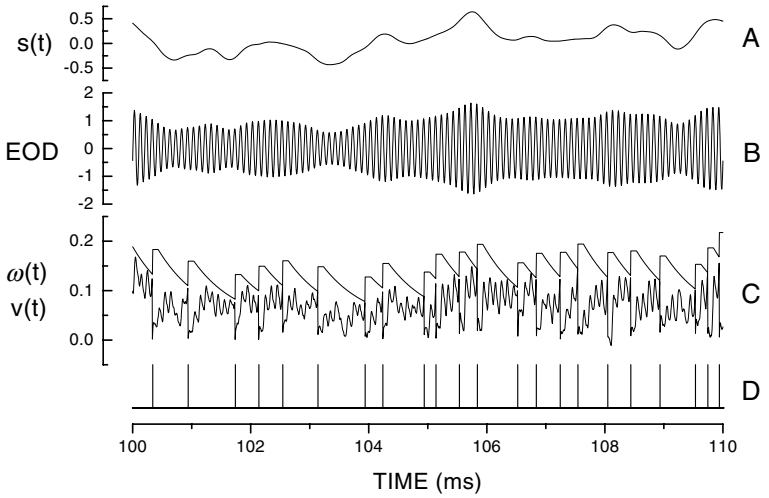

Fig. 2. Time series of various variables in the LIFDT model. (A) Signal that contains information about the fish's environment. (B) Transdermal potential due to the EOD (carrier) modulated by $S(t)$. (C) Resulting dynamics of the threshold $\omega(t)$ and potential $v(t)$ of LIFDT. (D) The output spike train of delta functions.

reduce the quality of encoding, because they break the one-to-one relation between the input amplitude and the output firing rate.

The dotted line of Fig. 3(A) was obtained with a non-zero multiplicative noise variance of $\sigma^2 = 0.0256$. It is clear from Fig. 3(A) that, apart from washing out the plateaus, noise does not affect the curve significantly. This is further illustrated in panels (B) and (C) where the mean P-value remains almost constant as either the intensity of multiplicative (B) or additive (C) noise increases.

Fig. 4(A) shows the ISIH in LIFDT without noise nor AMs; the model fires periodically every 5 EOD cycles (as in Fig. 1(A)). In panel B, a multimodal bell-shaped ISIH is obtained with synaptic

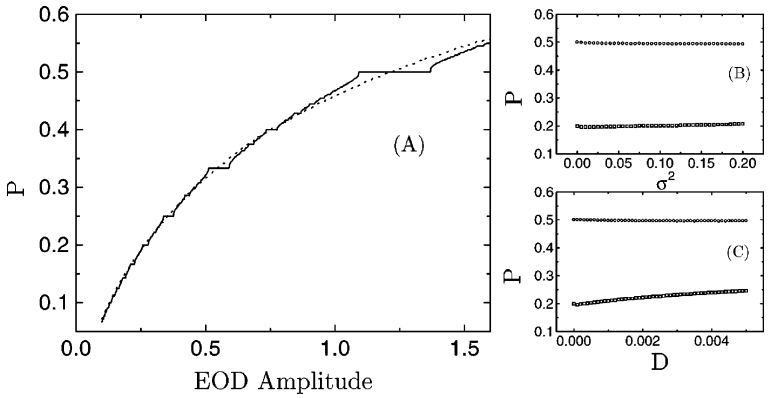

Fig. 3. P-value in LIFDT. (A) The firing probability per EOD cycle as a function of the mean EOD amplitude shows a devil's staircase shape in the deterministic case (—). Plateaus are wiped out by synaptic noise ($\sigma^2 = 0.0256$) ($\cdots$). Each point is evaluated from a 500 ms simulation. For typical amplitude values of synaptic (σ^2) (B) and additive ($D = \sigma^2_{\text{add}}\tau_{\text{add}}$) (C) noise used in our calculations, P is almost constant. EOD amplitudes are $r_0 = 0.261$ (□) and $r_0 = 1.2$ (○).

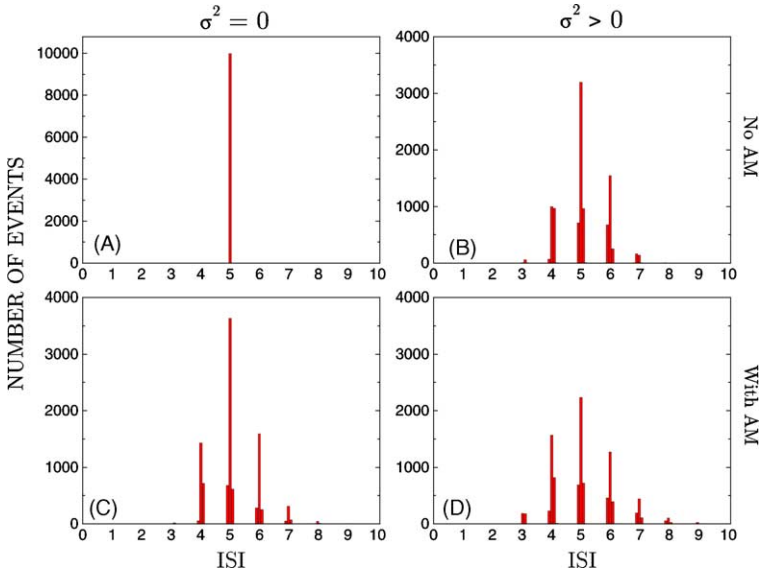

Fig. 4. Multimodal interval histograms in LIFDT. Top ISIH were computed without AMs while bottom graphics were made with AMs. No synaptic noise ($\xi(t)$ in Eq. (9)) was used for histograms on the left, while $\sigma^2 = 0.0256$ on the right. Note that time is in units of EOD cycles.

noise as seen experiments; the firing is no longer periodic and the intervals are spread over a few periods around the mean frequency (which stays at approximately 5 EOD cycles). Bottom panels were obtained using the same parameters but with a random AM on the EOD. Panel C shows the interesting fact that, even without noise, a multimodal ISIH is obtained in the presence of the AM alone, since the AM perturbs the deterministic periodic behavior. Finally, panel D shows the

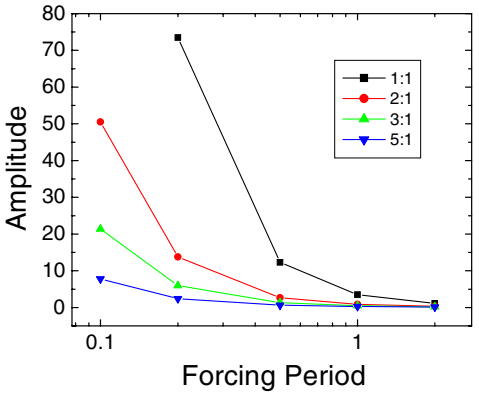

Fig. 5. Tuning curves of LIFDT. Each curve is obtained by finding the minimum amplitude giving rise to the indicated (n:m, or m spikes for n forcing cycles) firing pattern for different EOD forcing periods.

combined effect of both the AM and synaptic noise. The spread of the ISIH is greater than in the preceding cases.

Finally, tuning curves were calculated without AMs. This novel result is shown in Fig. 5. The shape of the 1:1 curve agrees with experiment [19]. This tuning curve was realized without internal noise, and we do not observe the V-shaped curves that we find in deterministic resonators. This suggests that the LIFDT itself has no preferential driving frequency.

5. Coding in the LIFDT model

We now present results on the effect of EOD amplitude and P-value on the coding fraction in the LIFDT model. The additive noise intensity D was set to zero; this did not affect our results qualitatively. One might expect the smoothing effect of P-unit noise (see Fig. 3(A)) to enhance the encoding of stimuli. The effect of increasing noise amplitude on the coding fraction actually depends on the mean EOD amplitude [2]. For example, in the 5:1 regime studied in the previous section ($P = 0.2$, $r_0 = 0.261$) increasing noise results in a lowering of the coding fraction. In this region the transfer function (Fig. 3) is already smooth enough for the AM to induce changes in the firing rate even without synaptic noise. Addition of noise simply randomizes the spike times and lowers the transmitted information. This is the case for most mean EOD amplitudes.

However, if the mean EOD is such that the dynamics are in a large phase locking plateau in Fig. 3), such as the 2:1 plateau, noise can enhance coding by breaking up the periodic phase-locked behavior. This was determined using a small enough stimulus so that without noise, the modulation is not strong enough to perturb the periodic phase locked pattern. The coding is then almost zero in the deterministic case. With increasing synaptic noise σ, the transfer function is smoothed out and the model starts coding. In other words, internal synaptic noise helps coding in this case. If σ^2 is too high, many irrelevant spikes are generated and the coding fraction decreases.

As the carrier mean amplitude r_0 increases, the firing rate increases monotonically in the presence of constant variance synaptic noise and AM. The increase translates into a better sampling rate of the input signal, thus into a greater coding fraction as shown in Fig. 6. The result

qualitatively agrees with measurements by Wessel et al. [16]: The coding fraction first increases and then saturates with increasing EOD amplitude. However, in Wessel et al. [16], the internal noise could of course not be changed as we do here. We also find that the curve associated with the larger noise amplitude has lower coding fraction.

From the known relation between the mean EOD amplitude r_0 and the P-value (measured without AM), the results of Fig. 6 are recast into a plot of the coding fraction vs P (Fig. 7). Again, we find an asymptotically increasing function which is also expected from the experiments in Wessel et al. [16]. What is of particular interest here is that for a given P-value, there is no unique value of the coding fraction. Thus P does not completely determine the quality of information

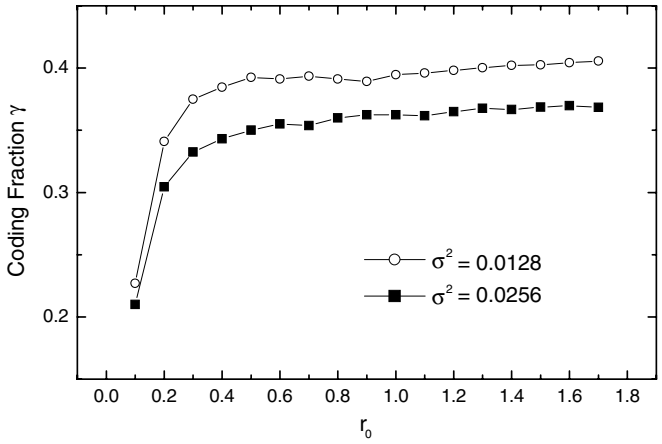

Fig. 6. Coding fraction vs r_0 in the LIFDT model.

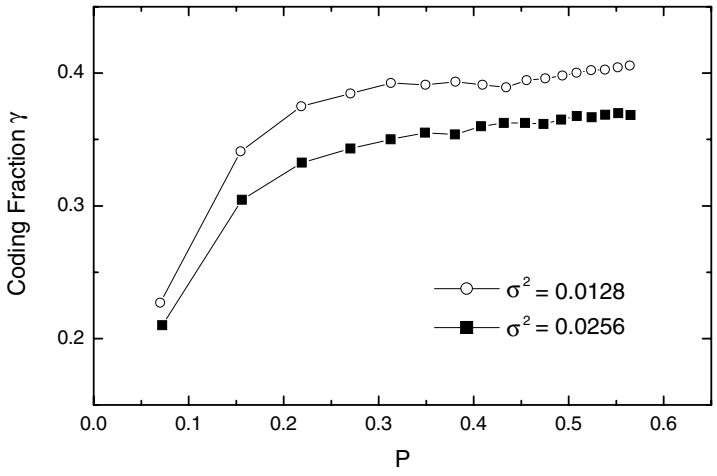

Fig. 7. Coding fraction vs P in the LIFDT model, for two values of synaptic noise variance. The results are from the same simulations as for Fig. 6; they are simply plotted as a function of P.

transfer in this model. It also depends on e.g. the synaptic noise strength and other model parameters.

6. Modulated point process model of P-units

The model investigated in this section was proposed in Nelson et al. [13], where the in vivo response of P-units to sinusoidal AMs of the (quasi-sinusoidal) EOD was studied as a function of the modulation frequency. This lead to a linear filter description of P-unit frequency response. This filter was then used to transform the stimulus $S(t)$ into a time-varying 'firing probability', which modulates the rate of a stochastic spike generator. Here we investigate the effects of the baseline firing rate and the spread of the interspike interval histogram on the encoding of AMs in this model. Note that this point process model class does not have noise-driven dynamics for the membrane voltage as in the LIFDT case. Nevertheless it reveals interesting coding features that are independent of such dynamics, such as the effect of mean firing rate and of threshold and saturation non-linearities.

6.1. Spiking mechanism in Nelson's model

The linear filter actually consists of three filters in parallel: two first-order high-pass filters and one constant gain filter. Two time constants τ_a, τ_b and three gain terms G_a, G_b and G_c parametrize the total filter, which in the Laplace domain is

$$H(s) = \frac{G_a s}{s + 1/\tau_a} + \frac{G_b s}{s + 1/\tau_b} + G_c, \tag{11}$$

where s is the complex frequency $(\mu + i\omega)$. The input stimulus is processed through the filter using Eq. (11). The filter output represents the modulation in P-unit firing rate. To this modulation, the mean firing rate – a constant term – is added to obtain a time-varying firing rate which fluctuates (due to the AM) around its mean. The filter output is fed to a clipping non-linearity, which produces both firing rate saturation (firing rate cannot exceed the EOD frequency f_{EOD}) and rectification (firing rate cannot be less than zero) observed in the P-units. The clipped rate is obtained by setting to zero any negative value of the rate, and by setting to f_{EOD} any value of the rate above f_{EOD}.

The stochastic spike generator is based on a uniform random number generator (see below). The model accurately describes the frequency response over the range of AM frequencies relevant to this fish [13]. However, we verified that it does not exhibit the autocorrelation seen in the P-unit data, nor can it reproduce the tuning curve since it is not driven by a sinusoidal EOD (only the AM modulates the rate).

6.2. Numerical implementation

Each set of simulations (differing by only one model parameter) used the same random stimulus, as in experiments [16]. The stimulus $S(t)$ was generated (like for the LIFDT model) using Eq. (4), see also [11], with $\alpha = 2\pi/10\ \mathrm{ms}^{-1}$. This signal was sent in parallel to the three filters, and also

stored with a sampling rate of 0.5 ms for coding fraction calculations. In the time domain, this amounts to numerically integrating

$$\dot{x}_a = -\frac{x_a}{\tau_a} + \frac{G_a}{\tau_a} S(t), \tag{12}$$

$$\dot{x}_b = -\frac{x_b}{\tau_b} + \frac{G_b}{\tau_b} S(t), \tag{13}$$

$$\dot{y} = -x_a - x_b + (G_a + G_b + G_c) S(t). \tag{14}$$

The parameters are $r_{\text{base}} = 300$ Hz, $\tau_a = 2.6$ ms, $\tau_b = 210$ ms, $G_a = 14.1$, $G_b = 0.47$, and $G_c = 0.67$. Simulations were performed using a stochastic Euler–Maruyama integration scheme with integration step $t = 0.005$ ms. The baseline firing rate of the neuron r_{base} was added to the summed output of these filters $y(t)$ so that the firing probability $r'(t)$ fluctuates around this mean value: $r'(t) = y(t) + r_{\text{base}}$. Since the model was built based on receptors of the species AL, as for our LIFDT model, a 'typical' value of the mean firing rate is 300 Hz. On the basis of this value, the amplitude of the incoming stimulus was chosen so that its filtered version (the non-clipped firing probability) had a standard deviation of 18% of the 300 Hz baserate, as in Wessel et al. [16]. The rate $r'(t)$ is then put through the clipping non-linearity, which produces the output firing probability $r(t)$. One can define a normalized time-varying spiking probability from the ratio $p(t) = r(t)/f_{\text{EOD}}$ which is bounded between 0 and 1.

Then a random uniform deviate β is generated at the end of each EOD cycle, and compared to the firing probability $p(t)$ at that time. If $\beta < p(t)$, a spike is triggered. A jitter is added to this time using a random Gaussian deviate, to match the observed phase locking (the width of ISIH modes). A Gaussian distribution with zero mean and standard deviation equal to 8% of the EOD period is sufficient to produce the desired jitter. Finally, an absolute refractory period equal to one EOD cycle is implemented by setting to the value of one EOD period any interval smaller than this period.

An enhanced version of the spike generator includes an additional parameter m that determines the spread of the ISIH [13]. At each EOD cycle, the program generates m Bernouilli trials (instead of only one as above), given the firing rate at that time. A spike is triggered only when m successful events are encountered, and we keep track of the number of positive results from one period to another. Suppose for example that at the first cycle, n of the m trials were successful. Then, if $(m - n)$ events are also successful at the next cycle, a spike will be triggered. If not, the cumulative number of successes is passed on to the third cycle, and so on. It is thus possible to change the spread without affecting the value of P (Fig. 8), and to study the effect of this spread on information transfer.

The spread of the ISIH (Fig. 8) can be quantified with the coefficient of variation (CV), i.e. the ratio of the standard deviation to the mean of the distribution. At $m = 1$, which corresponds to the basic version of the generator, the shape of the ISIH is similar to histograms observed in receptors driven by high-amplitude EODs [16]. As m is increased, the CV decreases since the mean does not change. At $m = 8$ the bell-shaped ISIH appears more like the histograms observed in the LIFDT model in the previous section.

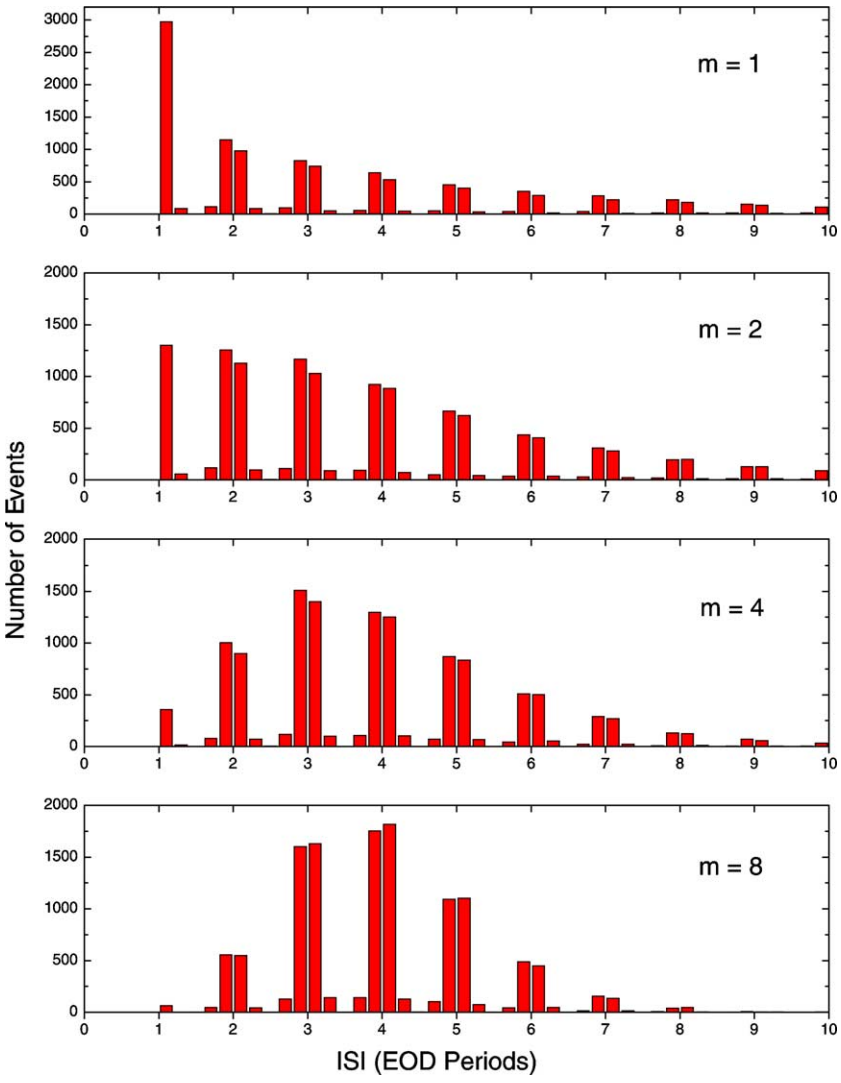

Fig. 8. Effect of m on the interspike interval histogram in Nelson's model. The average ISI has a value of 4 in all cases. Note that the top histogram is shown at a different scale due to the large number of short intervals.

The driving signal in the LIFDT model was implemented with constant contrast, i.e. with the mean EOD amplitude multiplying both the carrier and stimulus amplitudes. Here $S(t)$ is filtered and added to the constant r_{base}. The standard deviation of $S(t)$ is set so that the standard deviation of the probability modulation $y(t)$ is a fixed percentage of the mean probability r_{base}. For this contrast to be constant, whenever r_{base} is scaled from the 300 Hz value, the stimulus entering the filter must also be scaled by the same ratio. Thus, when r_{base} is increased, the amplitude of the input is also increased. And if $r_{\text{base}} = 0$, the input stimulus would also be set to zero. Our novel results below distinguish between the 'constant contrast' and 'constant stimulus' cases. In the latter case, the amplitude of the input remains fixed even if r_{base} changes.

6.3. Firing characteristics

Two parameters are of particular interest in Nelson's model for our study of stimulus encoding. The constant baserate r_{base} and the spread parameter m change the first and second moments of the ISIH, respectively. For zero stimulus, the output rate is equal to the baserate. The linear behavior of the firing rate vs baserate is shown by the diagonal line in Figs. 9 and 10. Here P is simply r_{base}/f_{EOD}. These figures also show the firing response for, respectively, the constant contrast and the constant stimulus versions of the model, for two stimulus intensities D_{st} (see Eq. (4)). It is observed that the firing rate deviates from the linear response when the baserate is near its extreme values 0 or f_{EOD}, and even more so for larger stimulus amplitudes. These regions are where the clipping non-linearity influences the rate $r(t)$.

A closer look at Fig. 9 for the constant contrast version shows firing rates that increase nearly linearly for $r_{base} \leqslant 600$ Hz or so. Such behavior is expected since the stimulus amplitude is scaled by the ratio $(r_{base}/300)$ which itself increases linearly starting from zero. Also, our stimulus has zero mean – and thus when averaged over the whole realization has no effect on the mean firing rate – which explains the nearly linear behavior of the firing rate in this region. However, non-linearity increases for larger r_{base}. When the baserate is near its maximum value, positive portions of the stimulus are clipped, and will not be encoded. The negative portions are not affected here, resulting in an overall negative deviation from linearity.

Fig. 9 shows that the firing rate as a function of the baserate for constant stimulus conditions is linear for midrange values of r_{base}, since small modulations have zero mean and do not affect the mean firing rate. However, the effect of the non-linearity is observed now at both ends of the graph and they are 'symmetric': The divergence at high rate towards smaller values of r_{base} is mirrored by the divergence at low rate towards greater values of r_{base}. The P value is not affected by r_{base}, but rather by the 'distance' of r_{base} from the linear regions. At high firing rates, the positive portions of the stimulus are clipped and P is reduced. Conversely, the negative portions of the

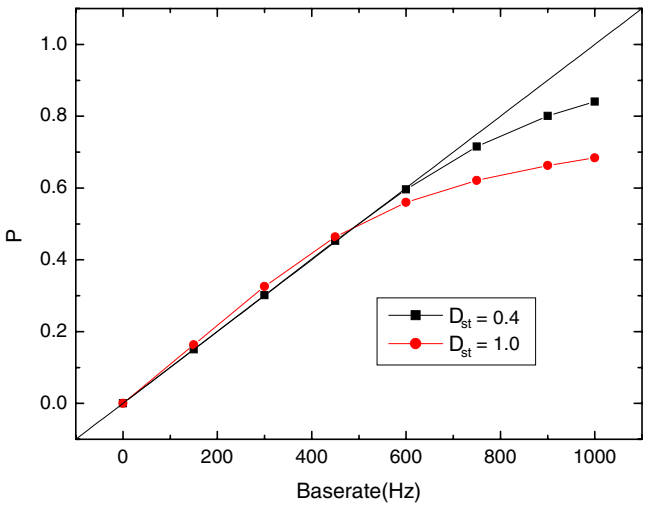

Fig. 9. P vs baserate in Nelson's model with constant contrast stimulation. Each point was obtained from the mean ISI of a 50 s simulation, following a 0.5 s transient.

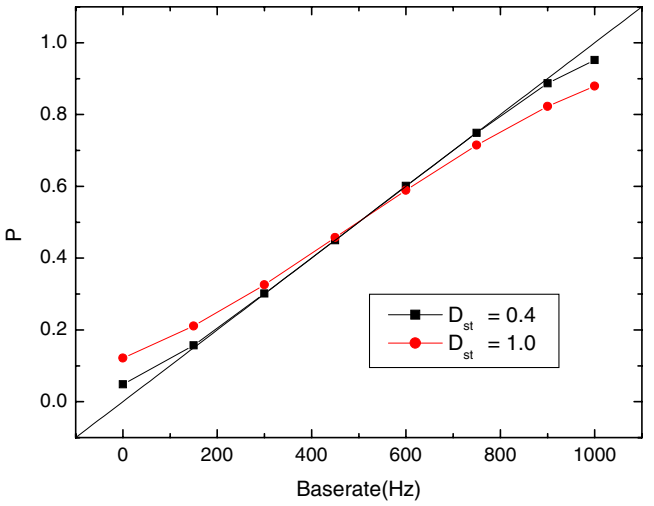

Fig. 10. P vs baserate in Nelson's model for two different 'constant stimulus' intensities. Details are the same as for Fig. 9.

stimulus are clipped at very low rate, thus increasing the P-value. Here again, the deviation is more important as the chosen stimulus amplitude is increased.

6.4. Results with Nelson's model

We present the effect of the baserate and m on the coding fraction and the mutual information in the Nelson model. These effects depend strongly on whether the amplitude of the input is kept constant, or scaled with the baserate (constant contrast). Here we set $m = 4$. According to Fig. 11 for the constant contrast case, the coding fraction and information rate are zero at zero baserate, since the stimulus is scaled to zero. As the stimulus amplitude is scaled with increasing baserate, the probability fluctuations become larger at the generator input. As a result the modulations are better encoded by the spike generator; the quality of the reconstruction and thus of information transfer increases with r_{base}. When r_{base} is large enough for the positive parts of the stimulus to be clipped, the coding fraction goes through a maximum and starts decreasing. As r_{base} approaches its maximal value, the lowered firing rate – negative fluctuations are no longer counterbalanced by positive ones (Fig. 9) – combined with the fact that nearly half the fluctuations are simply not encoded, produces a decrease in coding fraction.

The baserate being a constant value added to the spike generator input, it acts as a noise source that raises the baseline stochastic firing rate. From this point of view, the effect observed here is simply stochastic resonance in a modulated point process [17]. A moderate noise intensity first raises the firing rate, which results in a better encoding. We also observe an optimal value of the noise for which the coding fraction and information rate are maximum. Finally, the coding fraction decreases for high noise where random spiking dominates the response.

The behavior is very different for the constant stimulus case. With r_{base} set to zero, the negative portions of the modulation are clipped by the rectification. Nevertheless, its positive portions are encoded, resulting in a low yet non-zero coding fraction. Then for increasing baserate, the effects

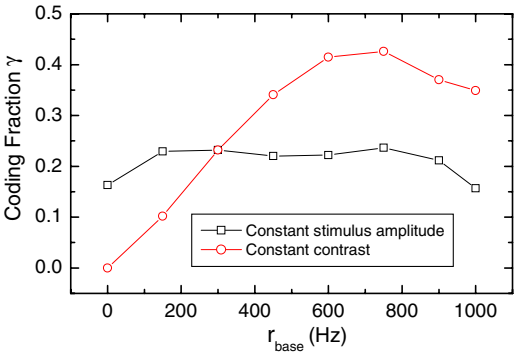

Fig. 11. Coding fraction and information rate vs baserate in Nelson's model.

of the rectification disappear, and information transfer increases. At the same time, the contrast between the stimulus amplitude and the baserate diminishes and more spikes start occurring at irrelevant times. When this latter effect becomes more important, both the coding fraction and information rate go through a maximum and start decreasing (around 300 Hz). Note that the curves for fixed stimulus amplitude are nearly symmetrical around 500 Hz. This suggests that the removal of spikes by negative fluctuations at high rate in this model has the same effect on encoding as the addition of spikes at low rates.

Information per spike as a function of the baserate is also very different for the two versions of the model (not shown). For constant stimulus, information per spike decreases monotonically as the baserate increases. The rapidly increasing number of spikes compared to the slowly varying coding fraction underlies this monotonic decrease. For constant contrast, each spike carries the maximum information around $r_{\text{base}} = 500$ Hz (half of f_{EOD}), right in the middle of the linear coding range, as expected.

The effect of m on the information transfer is presented in Fig. 12. As m increases, the fluctuations in the time intervals between successive spikes are averaged out and the model output

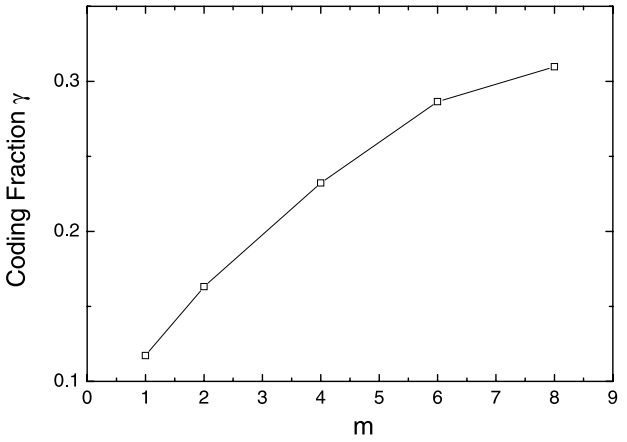

Fig. 12. Coding fraction, information rate and information per spike vs m in Nelson's model. $r_{\text{base}} = 300$ Hz.

becomes more regular (CV decreases, and the ISIH becomes narrower). As a result, the information transfer improves.

7. Discussion

The LIFDT model reproduces an important number of spike train statistics measured on P-unit receptors. The suprathreshold regime was considered in our study of weak AM encoding in this model, i.e. firings occur even without synaptic noise and EOD AMs. The model produces an inherent monotonic (except for a few phase locking plateaus) relation or transfer function between constant EOD amplitude and P-value; this relation is further smoothed out by noise. For the set of parameters in Chacron et al. [2] and which reproduce in vivo measurements, we found that the information transfer about AMs is almost always better without synaptic noise; adding noise only randomizes the spikes times and reduce coding quality. However, a beneficial effect of synaptic noise occurs when a small AM falls within a plateau of the $P - r_0$ relation. Its presence allows transitions to non-periodic firing patterns, thus allowing information from the stimulus to be encoded. This effect is reminiscent of yet different from stochastic resonance, since that effect involves subthreshold forcing.

Here we have found the important result that the quality of information is not completely determined by P. Two receptors with the same P-values may have different coding fractions, in particular if their associated ISIH are different. This is because P itself depends on the synaptic noise strength and other parameters such as the frequency of the EOD. We also investigated the quality of AM coding in a modulated point process model. Two variants of the models were investigated. In the first version, the stimulus was scaled with r_{base} ($\propto P$) to keep a constant contrast at the spike generator's input, as in the LIFDT model. It was found that the quality of the reconstruction increased with the baserate except near the saturation non-linearity where it started decreasing. In the second version, the stimulus was not scaled with r_{base}. We found that stimulus reconstruction quality behaved 'symmetrically' for the two manifestations of skipping: Information can be carried by either triggering spikes at low rates or by strategically preventing some spikes at high rates.

The enhanced version of the stochastic spike generator ($m > 1$) revealed interesting results by allowing the variation of the width of the ISIH without changing P. As m increased, the CV decreased, the model became more reliable, and each spike could carry more information for an overall beneficial effect on the transfer of information. The monotonically increasing curves in Fig. 12 mimick those observed in the simpler numerical model in Gabbiani and Koch [7,8] where the random-threshold integrate-and-fire model was used. In this latter 'Gestri' model, the value of the threshold is chosen randomly from a given distribution after each firing event. The CV can be set by adjusting the distribution from which random thresholds are picked. In Gabbiani and Koch [7,8], it was found that the coding fraction increased as the variability of the ISI distribution decreased, which is consistent with our findings.

We know that increasing the internal synaptic noise generally induces a shift of the ISIs to smaller values, but that it also makes the ISIH modes broader. Here we have shown how the important class of modulated point process models behaves from the point of view of coding, but also seen that, in order to get biophysical insight into what really influences coding quality,

dynamical models may be preferable. Both however predict to a similar extent that a higher mean firing rate is good for coding, at least in the linear regime.

Acknowledgements

This work was supported by NSERC Canada. We wish to thank Maurice Chacron and Len Maler for useful discussions.

References

[1] J. Bastian, Electrolocation 1. How the electroreceptors of *Apteronotus leptorynchus* code for moving objects and other external stimuli, J. Comp. Physiol. 144 (1981) 465.
[2] M.J. Chacron, A. Longtin, M. St-Hilaire, L. Maler, Suprathreshold stochastic firing dynamics with memory in P-type electroreceptors, Phys. Rev. Lett. 85 (2000) 1576.
[3] M.J. Chacron, A. Longtin, L. Maler, Negative interspike interval correlations increase the neuronal capacity for encoding time-dependent stimuli, J. Neurosci. 21 (2001) 5328.
[4] M.J. Chacron, K. Pakdaman, A. Longtin, Interspike interval correlations, phase locking and chaotic dynamics in a leaky integrate-and-fire model with dynamic threshold, Neural Comput. 15 (2003) 253.
[5] A.S. French, A.V. Holden, R.B. Stein, The estimation of the frequency response function of a mechanoreceptor, Kybernetik 11 (1972) 15.
[6] F. Gabbiani, Coding of time-varying signals in spike trains of linear and half-wave rectifying neurons, Network Comp. Neural Syst. 7 (1996) 61.
[7] F. Gabbiani, C. Koch, Coding of time-varying signal in spike trains of integrate-and-fire neurons with random threshold, Neural Comput. 8 (1996) 44.
[8] F. Gabbiani, C. Koch, Principles of spike train analysis, in: C. Koch, I. Segev (Eds.), Methods in Neuronal Modeling, 2nd Ed., MIT, Cambridge, MA, 2000, p. 313.
[9] J.P. Keener, F.C. Hoppensteadt, J. Rinzel, Integrate and fire models of nerve membrane response to oscillatory input, SIAM J. Appl. Math. 41 (1981) 127.
[10] B. Knight, Dynamics of encoding in a population of neurons, J. Gen. Physiol. 59 (1972) 734.
[11] A. Longtin, M. St-Hilaire, Encoding carrier amplitude modulations via stochastic phase synchronization, Int. J. Bifurc. Chaos 10 (2000) 2447.
[12] Z. Xu, J.R. Payne, M.E. Nelson, Logarithmic time course of sensory adaptation in electrosensory afferent nerve fibers in a weakly electric fish, J. Neurophysiol. 76 (1996) 13.
[13] M.E. Nelson, Z. Xu, J.R. Payne, Characterization and modeling of P-type electrosensory afferent responses to amplitude modulations in a wave-type electric fish, J. Comp. Physiol. A 181 (1997) 532.
[14] H. Scheich, T. Bullock, R.H. Hamstra Jr., Coding properties of two classes of afferent nerve fibers: high frequency receptors in the electric fish *Eigenmannia*, J. Neurophysiol. 36 (1973) 39.
[15] M.V. Tsodyks, H. Markram, The neural code between neocortical pyramidal neurons depends on neurotransmitter release probability, Proc. Nat. Acad. Sci. USA (1997) 719.
[16] R. Wessel, C. Koch, F. Gabbiani, Coding of time-varying electric field amplitude modulations in a wave-type electric fish, J. Neurophysiol. 75 (1996) 2280.
[17] K. Wiesenfeld, E. Pantazelou, J. Douglass, F. Moss, Stochastic resonance on a circle, Phys. Rev. Lett. 72 (1994) 2125.
[18] A. Zador, Impact of synaptic unreliability on the information transmitted by spiking neurons, J. Neurophysiol. 79 (1998) 1219.
[19] H.H. Zakon, The electroreceptive periphery, in: T.H. Bullock, W. Heilingenberg (Eds.), Electroreception, John Wiley and Sons, New York, 1986, p. 103.
[20] N. Berman, L. Maler, Neural architecture of the electrosensory lateral line lobe: adaptations for coincidence detection, a sensory searchlight and frequency-dependent adaptive filtering, J. Exp. Biol. 202 (1999) 1243.
[21] F. Gabbiani, W. Metzner, R. Wessel, C. Koch, From stimulus encoding to feature extraction in weakly electric fish, Nature 384 (1996) 564.